crystals

MDPI

Article

Sensing and Detection Capabilities of One-Dimensional Defective Photonic Crystal Suitable for Malaria Infection Diagnosis from Preliminary to Advanced Stage: Theoretical Study

Sujit Kumar Saini and Suneet Kumar Awasthi *

Department of Physics and Material Science and Engineering, Jaypee Institute of Information Technology, Noida 201304, India

* Correspondence: suneet_electronic@yahoo.com

Abstract: In the present research work we have examined the biosensing capabilities of one-dimensional photonic crystals with defects for the detection and sensing of malaria infection in humans by investigating blood samples containing red blood cells. This theoretical scheme utilizes a transfer matrix formulation in addition to MATLAB software under normal incidence conditions. The purpose of considering normal incidence is to rule out the difficulties associated with oblique incidence. We have examined the performance of various structures of cavity layer thicknesses 1000 nm, 2200 nm, 3000 nm and 5000 nm. The comparison between the performances of various structures of different cavity thickness helps us to select the structure of particular cavity thicknesses giving optimum biosensing performance. Thus, the proper selection of cavity thickness is one of the most necessary requirements because it also decides how much volume of the blood sample has to be poured into the cavity to produce results of high accuracy. Moreover, the sensing and detection capabilities of the proposed design have been evaluated by examining the sensitivity, figure of merit and quality factor values of the design, corresponding to optimum cavity thickness.

Keywords: photonic crystals; biosensors; transfer matrix method

Citation: Saini, S.K.; Awasthi, S.K. Sensing and Detection Capabilities of One-Dimensional Defective Photonic Crystal Suitable for Malaria Infection Diagnosis from Preliminary to Advanced Stage: Theoretical Study. *Crystals* **2023**, *13*, 128. https://doi.org/10.3390/cryst13010128

Academic Editor: Alessandro Chiasera

Received: 5 December 2022
Revised: 4 January 2023
Accepted: 7 January 2023
Published: 11 January 2023

1. Introduction

The pioneering research work on photonic crystals (PCs) by two scientists, Yablonovitch and John in 1987, has revolutionized the research field of optical engineering and technology [1,2]. PCs have commendable control of the propagation of light passing through them. The periodic modulation of refractive indices of the constituent materials of PC results in the formation of photonic band gap (PBG) due to Bragg scattering of incident waves from the interfaces between the various material layers of the structure [3,4]. PBG restricts the propagation of light of specific frequencies from the structure and allows the propagation of light of other frequencies to pass through. PCs can be classified into three categories, depending upon the modulation of the refractive index of the constituent materials in x, y and z directions as one-dimensional (1D), two-dimensional (2D) and three dimensional (3D) PCs. The ease of fabrication techniques associated with 1D PCs motivated the photonic engineers to explore the biosensing capabilities of 1D photonic structures with a defect. In recent years, the rapid, advanced and accurate biosensing capabilities of 1D defective photonic crystal (DPC) have attracted the attention of photonic technocrats to design and develop photonic biosensors due to their importance in the field of applied sciences, such as for security, medical, defense, food detection, environment, and aerospace worldwide [5]. Actually, the creation of an empty space known as a cavity region inside photonic structures is responsible for the break in periodicity which results in the existence of a sharp tunneling peak inside the PBG of the structure. The optical properties of the tunneling peaks (also

called the defect mode) are strongly dependent upon both the refractive index and the thickness of the cavity region. This property of the defect mode is very useful in designing various biosensors consisting of 1D DPCs [6–8]. For example, Zaky et al. suggested a plasma cell sensing device based on 1D DPC for the detection and sensing of convalescent plasma whose refractive index variation is restricted between 1.3246 and 1.3634 [9]. Another photonic design capable of detecting glucose concentration levels has been investigated by Asmaa et al. Their design works on the principle of Fano-resonance, which is excited across the interface between PC and metallic capping mounted on top of the structure [10]. In contrast to the conventional biosensing technologies based on plasmonics and photonic crystal fibers, 1D DPC based biosensors are highly sensitive sensing mechanisms due to the ultra-high localization of light inside the cavity region. Additionally, 1D DPC based biosensing lowers down the volume requirement of the sample under investigation [11]. Moreover, 1D DPC based sensors are compact in size and easily accommodated in a complex environment [12]. Moreover, the compatibility between 1D photonic structures and integrated photonic circuits encourages their extensive role in the fields such as force–strain, temperature, liquid, pressure, displacement, gas and biomedical engineering [13–15].

Nowadays, blood examination is an essential tool for identifying hematological disorders which are responsible for a series of non-communicable diseases such as diabetes, coronary artery, cancerous and respiratory [16]. As per the report of the World Economical Forum, published in September 2011, these diseases were the root cause of around 36 million mortalities across the world [17]. Therefore, examining the human blood sample is one of the cheapest, most necessary and easiest ways to carry out regular and periodic health monitoring. The blood sample examination helps in identifying the diseases and become a foundation for proper treatment. Human blood is made up of a large number of bio-constituents which are approximately more than 4000 in number [18]. Actually, nowadays, blood optics play an important role in biophotonic sensing and clinical therapy applications [19]. The absorption and scattering characteristics of light interacting with the blood sample depend on the refractive index of the erythrocytes present in the blood sample, which is strongly dependent upon the hemoglobin concentration of erythrocytes [20]. Blood is a highly functional bodily fluid whose refractive index is complex in general [21]. More than half of human blood is made up of blood plasma, which contains various proteins such as red and white blood cells, enzymes, albumin, hormones, glucose, minerals, etc. [22] The supply of oxygen from lungs to different body parts is being accomplished by hemoglobin, also known as a main protein present in red blood cells (RBCs). On the other hand, white blood cells (WBCs) which are also known as leukocytes, strengthen our body to fight against various infections [23]. The dielectric properties of human blood have great relevance in various medical applications such as early stage detection of cancer cells in the human body and several other diseases. For example, the dielectric blood coagulometry helps us to analyze the whole spectra of human blood to understand the biological, physical and chemical properties comprehensively [24].

Malaria is one of the fatal diseases caused by protozoan parasites of the genus plasmodium [25,26]. Untreated or misdiagnosed malaria may become a root cause of death globally. According to the World Health Organization (WHO), around 405,000 casualties out of 228 million malaria cases were reported in 2018 worldwide [27]. If someone is bitten by female anopheles mosquito protozoan, parasites enter into the red blood cells of the human body through the liver [28]. The presence of protozoan parasites in the RBCs results in structural and biological change in RBCs. This modification degrades hemoglobin, which is the main constituent of RBCs. This degradation of hemoglobin becomes nutrition for protozoan parasites. These parasites digest hemoglobin of the human body as a free ferrous heme, which is quickly transformed into ferric heme and are highly toxic. This transformation results in the change in the homogeneous structure of RBCs. Malaria diagnosis must be speedy, reliable and very accurate for their eradication via timely treatment [29,30]. At present, various conventional approaches are being used in malaria diagnosis, and all of these conventional approaches have limitations due to

their laboratory requirements and/or the complexity involved in investigation. Some other limitations associated with the conventional approaches are sample size requirement, sensitivity, result accuracy, time-consumption and difficulties associated with early-stage detection of malaria, depending upon the stage of infection [31]. On the other hand, 1D photonic biosensors can satisfactorily address all the above issues pertaining to timely and early-stage detection of malaria infection in humans. Moreover, investigations conducted by 1D photonic biosensors are rapid and cost effective, which brings the medical expenses within the reach of poorer people. For example, Somaia et al. explored the biosensing application of 1D PC by studying the propagation of a p polarized wave through 1D PC. They have shown a 714% improvement in the sensitivity of the structure as compared to the waveguide based conventional sensors [32]. Both Mahdi et al. and Taya have exploited the defect mode properties of 1D ternary photonic structure for minute refractometric sensing application loaded with the various analytes having refractive index variation between 1.00 to 1.06 and 1.33 to 1.35, respectively [33,34]. In addition, Banerjee has suggested how a 1D ternary photonic structure can be used as an enhanced sensitivity gas sensor [35]. The surface plasmon resonance driven photonic crystal fiber based biosensing structures are suggested by research groups of Qingli et al. and Zhiwen et al. [36,37]. Tongyu et al. suggested the PC cavity coupled photonic sensor for simultaneously sensing refractive index and temperature by using an electromagnetically induced transparency effect [38]. Recently, Zina et al. suggested how 1D PC consisting of cold magnetic plasma and quartz materials according to the Copper mean sequence can be used for the detection of the magnetic field direction by studying the external magnetic field dependent movement of ultra large PBG of the structure [39]. Parandin et al. suggested a 2D photonic biosensor made up of circular nano-rings between the waveguides for the detection of various blood components [40,41]. Liu et al. demonstrated how a 2D PC based cavity structure can be used as a quality sensor for the detection of ethanol [42]. Olyaee et al. designed a pressure sensor composed of a 2D PC of ultra-high sensitivity and resolution, by performing finite difference time domain simulation [43]. Moreover, Claudia has suggested how porous silicon material based photonic biosensing structures can be used as high performance sensors [44].

The present work is focused on the biosensing properties of 1D DPC for the diagnosis of various stages of malaria infection present in human body. The organization of the present manuscript is as follows. Section 2 deals with the structural design of the proposed work. Theoretical formulation is discussed in Section 3. The results of this work are given in Section 4. Section 5 deals with conclusions of the proposed work.

2. Structural Design

Figure 1 represents the structural design of the present blood sensor composed of 1D DPC for the detection of various stages of malaria infection. The present biosensing structure $(AB)^{N}C(AB)^{N}/GS$ can easily be fabricated by creating a defect layer C of air at the middle of the 1D PC composed of alternating layers A and B of materials: silicon (Si) and lanthanum flint (LAFN7), respectively. The alphabet N represent the period number of the structure. The ion-bean sputtering technique can be used for the fabrication of the proposed biosensing structure composed of Si and LANF7 on glass substrate for the detection of malaria infection through red blood cell (RBC) samples containing Cell A, Cell B, Cell C, Cell D and Cell E separately [45–47].

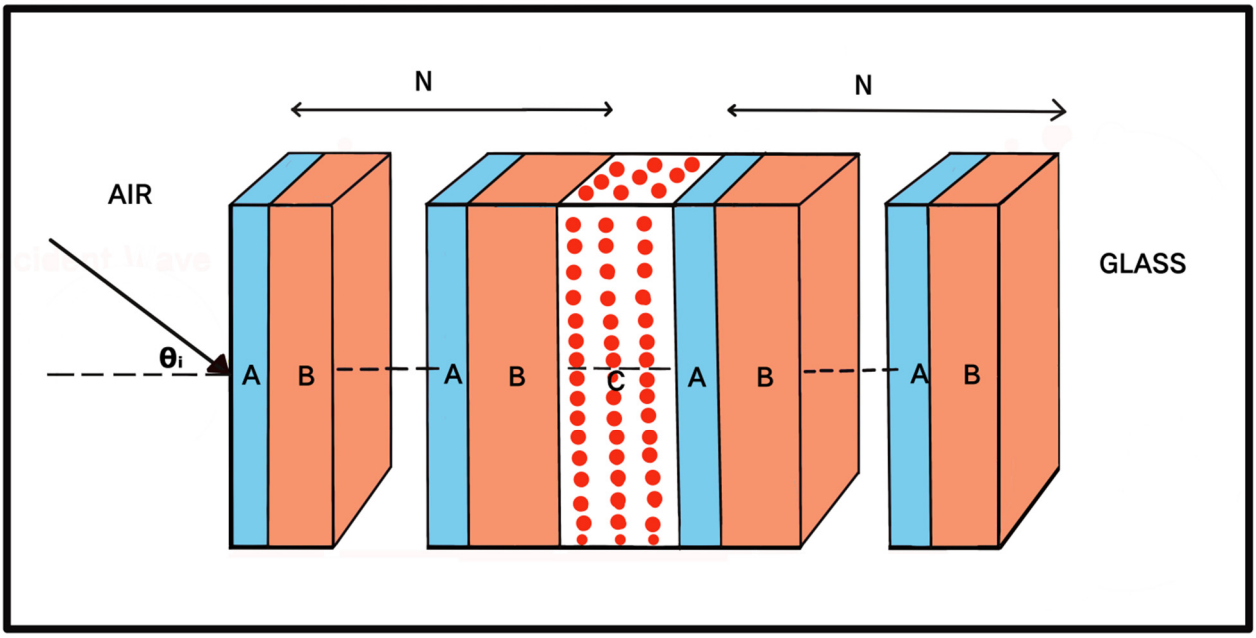

Figure 1. Schematic view of the proposed blood sensor for malaria detection and sensing composed of 1D photonic crystal with single defect.

3. Theoretical Formulation

In order to obtain the simulation results through MATLAB software, we have used a transfer matrix method [48,49]. This is one of the most suitable techniques for the computation of simulation results of the proposed 1D photonic biosensing structure. According to this method, the amplitudes of electric and magnetic fields associated with incident and transmitted electromagnetic radiation at either ends of the structure, i.e., incident and transmitted ends, are connected via transfer matrix as

$$Z = (z_1 z_2)^N z_3 (z_1 z_2)^N = \begin{pmatrix} Z_{11} & Z_{12} \\ Z_{21} & Z_{22} \end{pmatrix} \quad (1)$$

Here, Z_{11}, Z_{12}, Z_{21} and Z_{22} are representing the elements of resultant transfer matrix Z. The z_1, z_2 and z_3 are being used for representing the characteristic matrix of layers A, B and C, respectively [50].

The coefficient of transmission t of the proposed biosensing structure [air/(Si/LAFN7)^N/cavity/(Si/LAFN7)^N/GS] is defined as

$$t = \frac{2p_0}{(Z_{11} + Z_{12}p_s)p_0 + (Z_{21} + Z_{22}p_s)} \quad (2)$$

Here, $p_0 = n_0 \cos(\alpha_0)$ and $p_s = n_s \cos(\alpha_s)$ are corresponding to input and exit ends of the structure, respectively, for s-polarized wave. For p-polarized wave, $p_0 = \cos(\alpha_0)/n_0$ and $p_s = \cos(\alpha_s)/n_s$. Additionally, α_0 and α_s are representing angles of incidence and emergence in incident and exit media, respectively.

Finally, the transmittance $\Im$ of the proposed biosensing structure is

$$\Im = \frac{s_s}{s_0}|t|^2 \times 100 \quad (3)$$

4. Results and Discussions

The transfer matrix method as discussed above has been applied over the proposed 1D defective photonic structure (AB)^{N}C(AB)^N/G as presented in Figure 1. We have used MATLAB software to obtain the transmittance of the proposed biosensor under normal

incidence conditions. The purpose of considering the normal incidence is to overlook the challenges associated with the oblique incidence, along with the requirement of transverse electric and transverse magnetic modes of incident light. The entire simulations have been carried out in the visible region of the electromagnetic spectrum, extending from 600 nm to 700 nm. The materials silicon (Si) and lanthanum flint (LAFN7) have been used to fabricate the layers *A* and *B* of the proposed 1D multilayer stack of refractive indices, n_{Si} = 3.5 and n_{LAFN7} = 1.7, respectively, on the glass substrate of refractive index n_s = 1.57. The purpose of selecting Si and LAFN7 materials in our design is to ensure a large refractive index contrast between the high and low refractive index layers of the proposed structure, which is one of the essential requirements for getting wider as well as deeper photonic band gap (PBG). The depth of the PBG may also be increased by increasing the period number. However, instead of increasing the period number of the design, we have preferred to ensure large refractive index contrast to obtain wider PBG. The wider PBG also increases the possibility of having a large number of resonant transmission peaks whose central wavelengths are restricted inside the PBG of the structure. Moreover, larger PBG also improves the number of blood samples to be investigated by our design, depending upon their refractive index variation. In the present work the refractive index variation between the blood samples is from 1.371 to 1.408 depending upon the stages of malaria infection (Table 1). In this simulation work, the thicknesses of layers *A* and *B* are taken as d_A = 70 nm and d_B = 400 nm. The period number *N* has been fixed to 10. The defect layer of thickness *dd* = 300 nm has been created at the middle of the proposed biosensor by disturbing the periodicity of the design, as shown in Figure 1.

Table 1. Refractive index values of various cells depending upon the hemoglobin concentration within RBCs [28].

Stage of Infection	RBC Component	Refractive Index	Hemoglobin Concentration (g/dL)
Healthy	Cell A	1.408	30.9
Ring	Cell B	1.396	25.59
Trophozoite	Cell C	1.381	19.78
Schizont	Cell D	1.372	16.28
Schizont	Cell E	1.371	15.9

4.1. Description of Malaria Samples Used

In this study, we have investigated four samples of malaria-infected red blood cells (RBCs) as B, C, D and E cells with respect to the sample containing healthy RBCs, referred as cell A. Here, cells B, C, D and E correspond to different stages of malaria infections with respect to cell A, which represents the healthy stage. Table 1 gives the refractive index of values of samples containing healthy and malaria infected RBCs obtained by Agnero et al. [51]. They suggested an optical method based on the transportation of the intensity equation which differentiates between malaria infected and healthy RBCs by combining the topography, three dimensional reconstruction of refractive index and deconvolution of RBCs. Actually, RBCs are a mixture of 32% of hemoglobin surrounded by 3% membrane and 65% water [52]. RBCs can be considered as an aqueous solution in which hemoglobin is dissolved. Both Kevin and Tycko et al. suggested that the change in the hemoglobin concentration within RBCs results in the significant change in the refractive index of cells as shown in Table 1 [53,54]. The refractive index and hemoglobin concentration within RBCs are the two essential parameters which are usually used to identify whether or not RBCs belong to a healthy or malaria infected person.

In healthy RBCs, hemoglobin is one of the major of components of cells. These healthy cells are physically identified by their biconcave shape, whose edges are thicker than the middle. The main function of RBCs is to maintain flow of oxygen and carbon dioxide inside the human body. Hence, if RBCs are healthy, it means the flow of O_2 and CO_2 inside body is perfect. For healthy RBCs, the range of hemoglobin concentration of cell A

should be between 28 g/dL and 36 g/dL, which corresponds to refractive index values between 1.402 and 1.409, respectively [28]. If someone is bitten by the female Anopheles mosquito, parasites enter into the body and reach the RBCs through the liver. The presence of parasites in RBCs initiates the biochemical and structural changes of host cells due to which homogeneous structure of cell is lost. Moreover, the presence of parasites into the cells also decreases both the hemoglobin concentration and refractive index value of that cell. Therefore, the presence of parasites within the various cells is ensured by the region having a low refractive index [28–30]. This is the first stage of malaria infection and is called the ring stage. In this stage, the shape of the RBC remains biconcave and the infected cell is named as cell B. After the ring stage, the malaria infection reaches the trophozoite stage. In this stage, parasites are mature enough and have a more intense metabolism because host cells *C* lost their biconcavity. Finally, infection reaches to its prominent stage, called the schizont stage. In this stage, the growth of the parasites reaches to an advanced level and the corresponding infection is called cell D. By knowing the refractive index and concentration of the cell in the RBCs, one can easily identify the schizont stage of malaria infection by means of an optical route. Generally, the refractive index and hemoglobin concentration of quasi-identical cells D and E are different even though both are representing the same stage of infection, as shown in Table 1 [25–30].

We have also performed the linear curve fitting, as shown in Figure 2, over the data given in Table 1, to extract an expression which gives the hemoglobin concentration (C_{Hb}) inside RBCs corresponding to the refractive index (n_{RBC}) of the samples depending upon the distribution of cell. It can be clearly seen from Figure 2 that the increase in the refractive index of the cell is due to the increase in the hemoglobin concentration within RBC samples. The red line in Figure 2 is representing a liner curve fitting equation obtained from simulated data. The change in hemoglobin concentration within RBCs can easily be obtained by putting the value of n_{RBC} in the curve fitting equation given below:

$$C_{Hb} = 402.35 n_{RBC} - 535.8 \left(R^2 = 0.9992 \right) \quad (4)$$

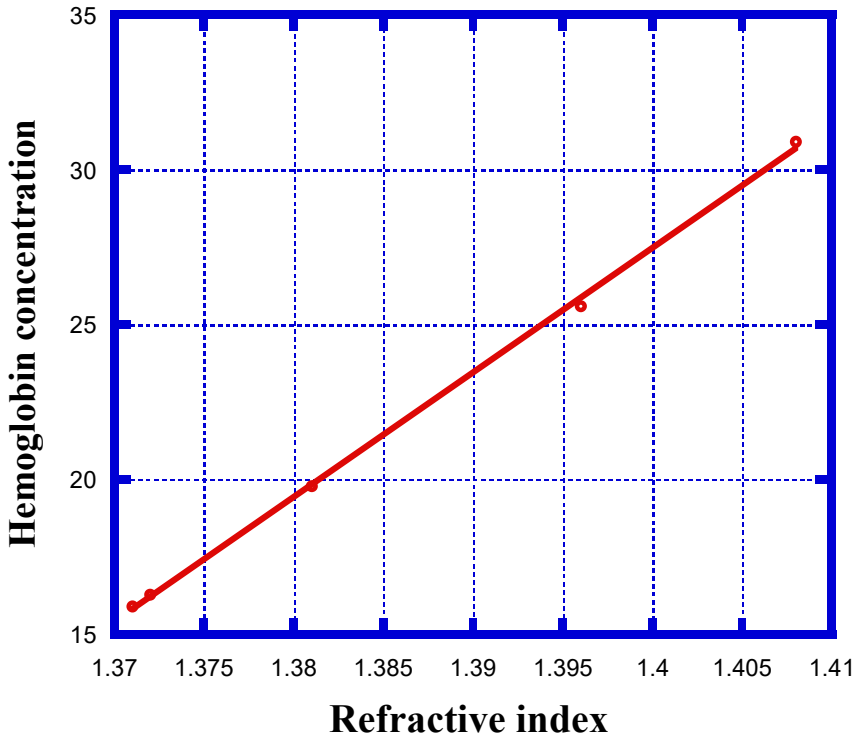

Figure 2. The diagram showing refractive index of RBC components containing cells A, B, C, D and E dependent upon the hemoglobin concentration of blood.

Here, R^2 represents the square of the correlation coefficient which determines the accuracy between the simulated and curve fitting data. The higher value of R^2 is always accepted to validate the results.

4.2. Initialization of Biosensing Application of the Proposed Design Loaded with Water Sample

The empty space of the defect layer is infiltrated by a pure water sample of refractive index 1.333 to initiate the biosensing application of the design. The infiltration of the water sample into the cavity of the proposed biosensor results in the confinement of light into the cavity region. This confinement of light appears as a defect mode of unit transmission inside the photonic band-gap of the structure located at 620.9 nm, as shown in Figure 3.

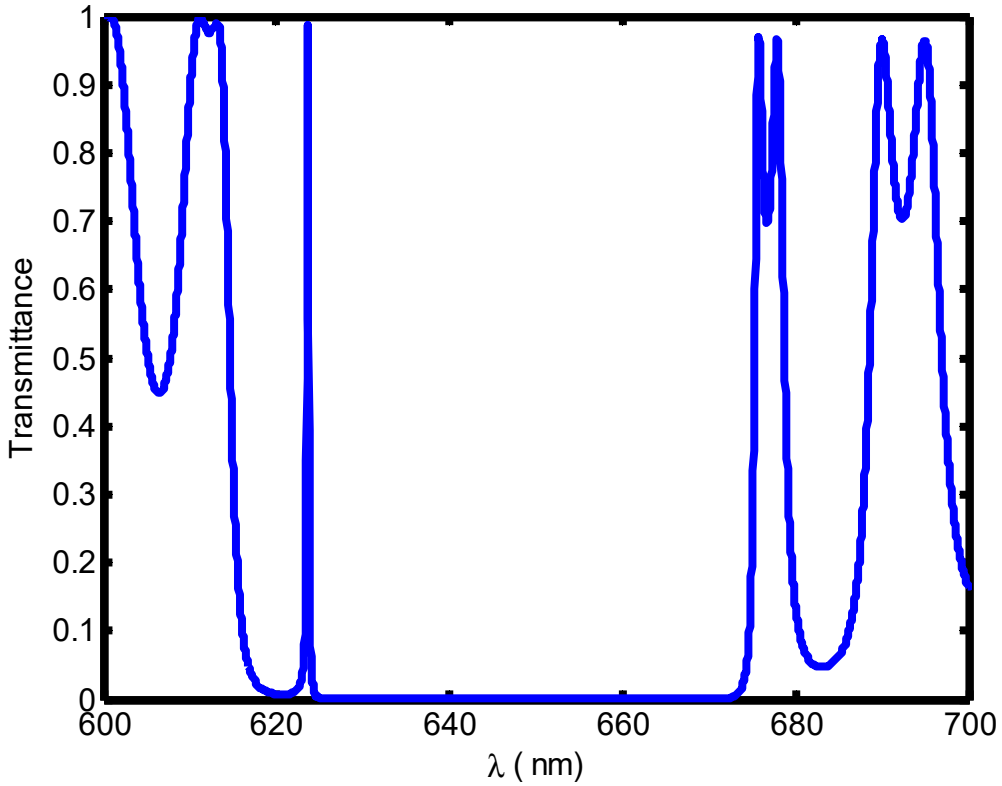

Figure 3. Transmission spectra of proposed biosensor loaded with water sample corresponding to cavity of thickness *dd* = 300 nm at normal incidence.

For analyzing the performance of the proposed design one may use the approach suggested by us. Firstly, both the ends of the biosensor are connected with single mode fiber (SMF) through precision positioning equipment to avoid errors during measurements. The light from the polychromatic source is launched into the structure via the input end of the design through SMF. The output terminal of the proposed design is connected with the optical spectrum analyzer (OSA) through SMF for the projection of the biosensing results into the monitor via computer. The qualitative setup for analyzing the performance of the proposed biosensing is shown in Figure 4, below, as per our understanding, though the findings of the proposed work are based on theoretical simulation which has been carried out with the help of the transfer matrix method in addition to MATLAB software.

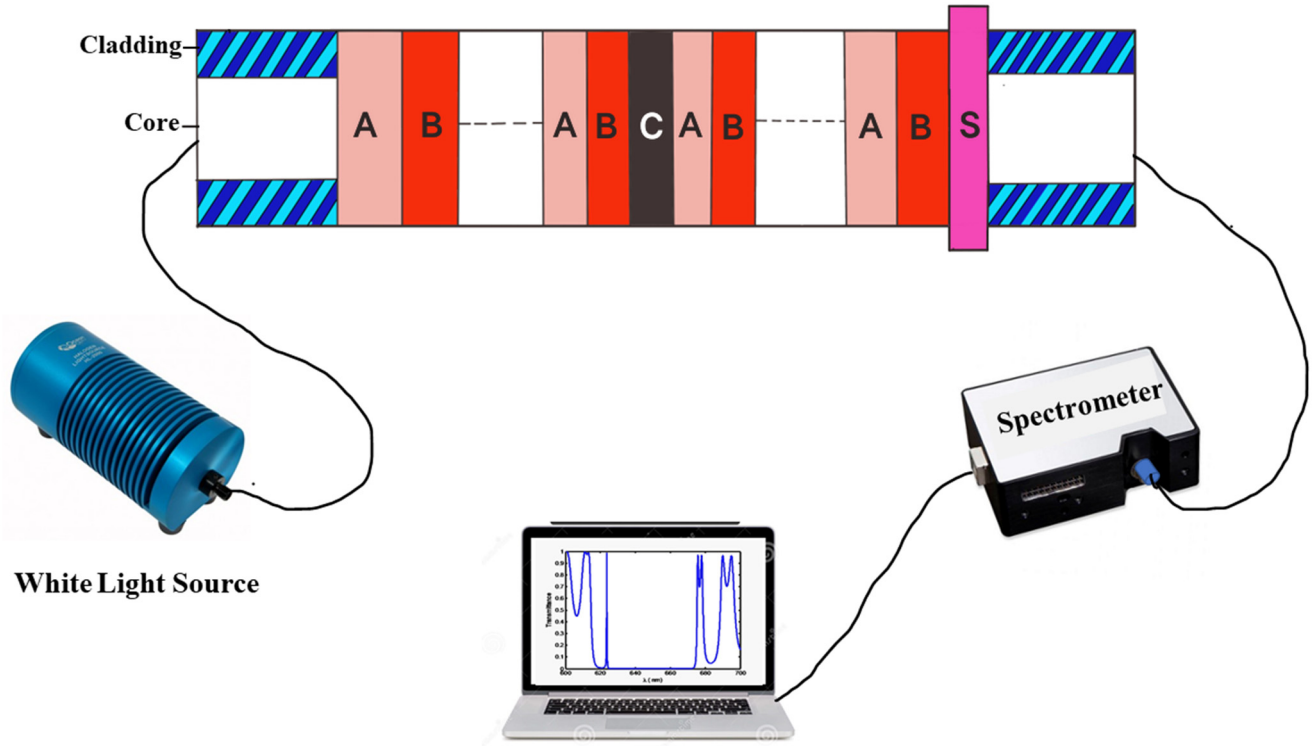

Figure 4. Experimental setup is required for the measurement of transmission response of the biosensor. Here, letters A, B and C represent silicon, lanthanum flint and air layers of the structure fabricated on the glass substrate S.

4.3. Evaluation of Biosensor Performance Loaded with Different Blood Samples

In this section, we are highlighting the biosensing capabilities of the proposed design loaded with hemoglobin blood samples containing Cell A, Cell B, Cell C, Cell D and Cell E, one at a time for the diagnosis of malaria infection. Figure 5, below, shows the transmission spectra of the proposed biosensor loaded with different five RBC samples under examination. The defect mode peaks of unit transmission shown in blue, black, red, yellow and purple solid line colors are corresponding to RBC samples containing Cell A, Cell B, Cell C, Cell D and Cell E, respectively, under investigation. After recording the central wavelength of each defect mode inside PBG with the help of the setup described above, we have calculated the sensitivity of the design of cavity thickness dd = 1000 nm with the help of the following equation [6–11]:

$$S = \frac{d\lambda}{dn}(\text{nm/RIU}) \tag{5}$$

Here, $d\lambda$ is representing the change in the position of central wavelength of the defect mode associated with the particular sample with respect to the water sample, and dn is the corresponding difference between the refractive index of that sample with water.

The proposed biosensor could achieve a maximum sensitivity value of 148.1 nm/RIU, corresponding to defect layer thickness dd = 1000 nm. A high value of sensitivity is always desirable for the designing of any high performance photonic biosensor, so we have given our efforts to improve the sensitivity further. For this purpose, we have randomly chosen some higher values of cavity thickness such as dd = 2200 nm, 3000 nm and 5000 nm, also keeping all other parameters of the design fixed as discussed above. The transmission spectra of the proposed biosensing structures corresponding to defect layer thicknesses dd = 2200 nm, 3000 nm and 5000 nm are plotted in Figures 6–8, respectively.

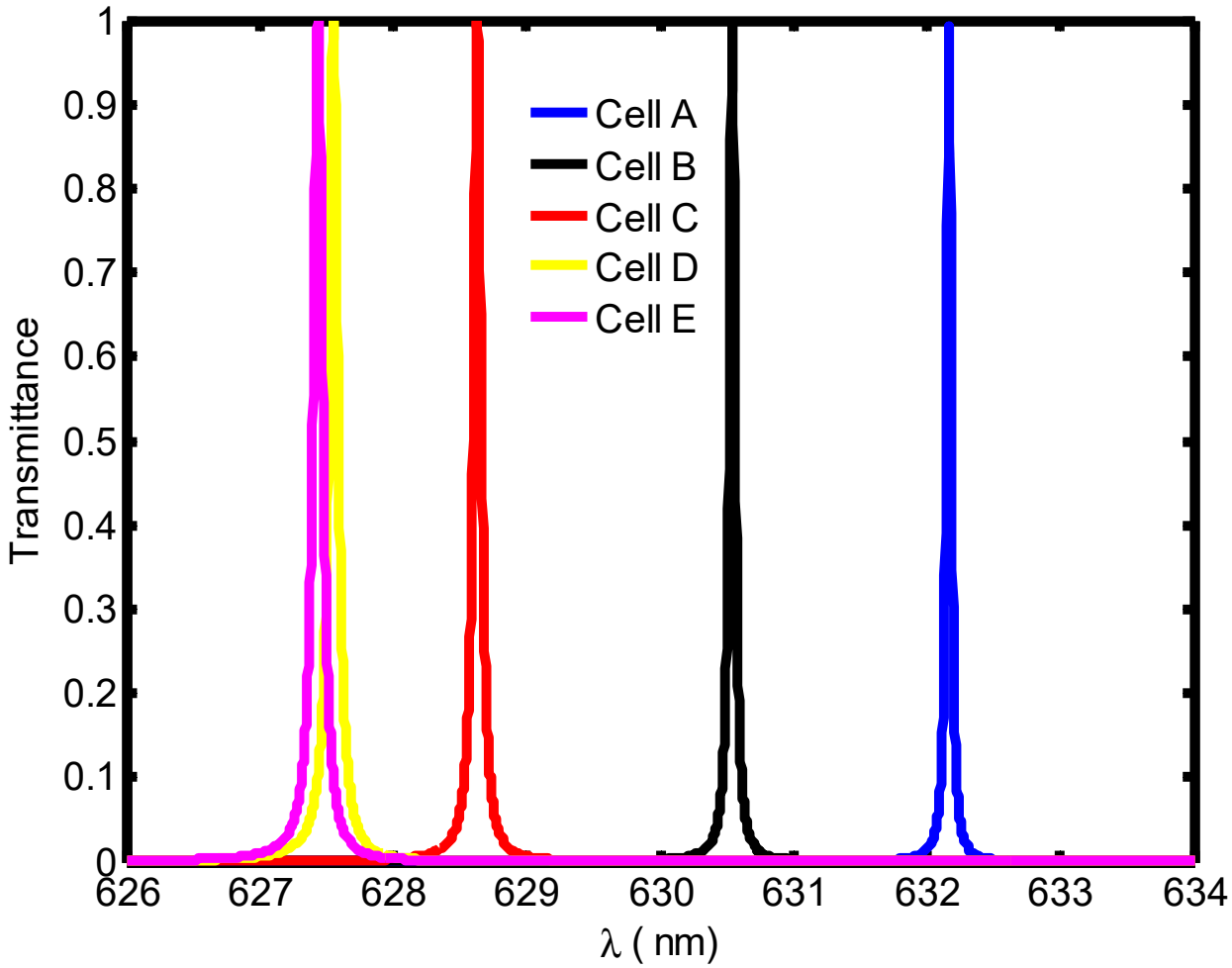

Figure 5. Transmission spectra showing five defect modes in solid blue, black, brown, yellow and purple line colors corresponding to RBC sample containing A, B, C, D and E blood cells separately, one at a time. The thickness of cavity layer is *dd* = 1000 nm under normal incidence.

The comparison of Figures 5–8 shows that as the defect layer thickness increases, the defect modes corresponding to all five samples show red shifting. This shifting is between wavelength range 626 nm to 633 nm corresponding to *dd* = 3000 nm and 658 nm to 675 nm corresponding to *dd* = 5000 nm, respectively. Further increase in the defect layer thickness results in the movement of defect modes beyond 665 nm, i.e., outside the PBG extending from 620 nm to 665 nm (Figure 3). There is one more common observation, that, corresponding to defect layer thickness 2200 nm, 3000 nm and 5000 nm, the intensity of all defect modes associated with the five samples is slightly reduced. However, this reduction does not affect the performance of the design, due the fact that the reduced intensity of defect modes is significantly higher in comparison to the threshold limit of the OSA, which is used for the detection of defect modes under the influence of different RBC samples. The numeric values of the sensitivity of the proposed designs corresponding to cavity thickness *dd* = 1000 nm, 2200 nm, 3000 nm and 5000 nm have been summarized in Table 2 below.

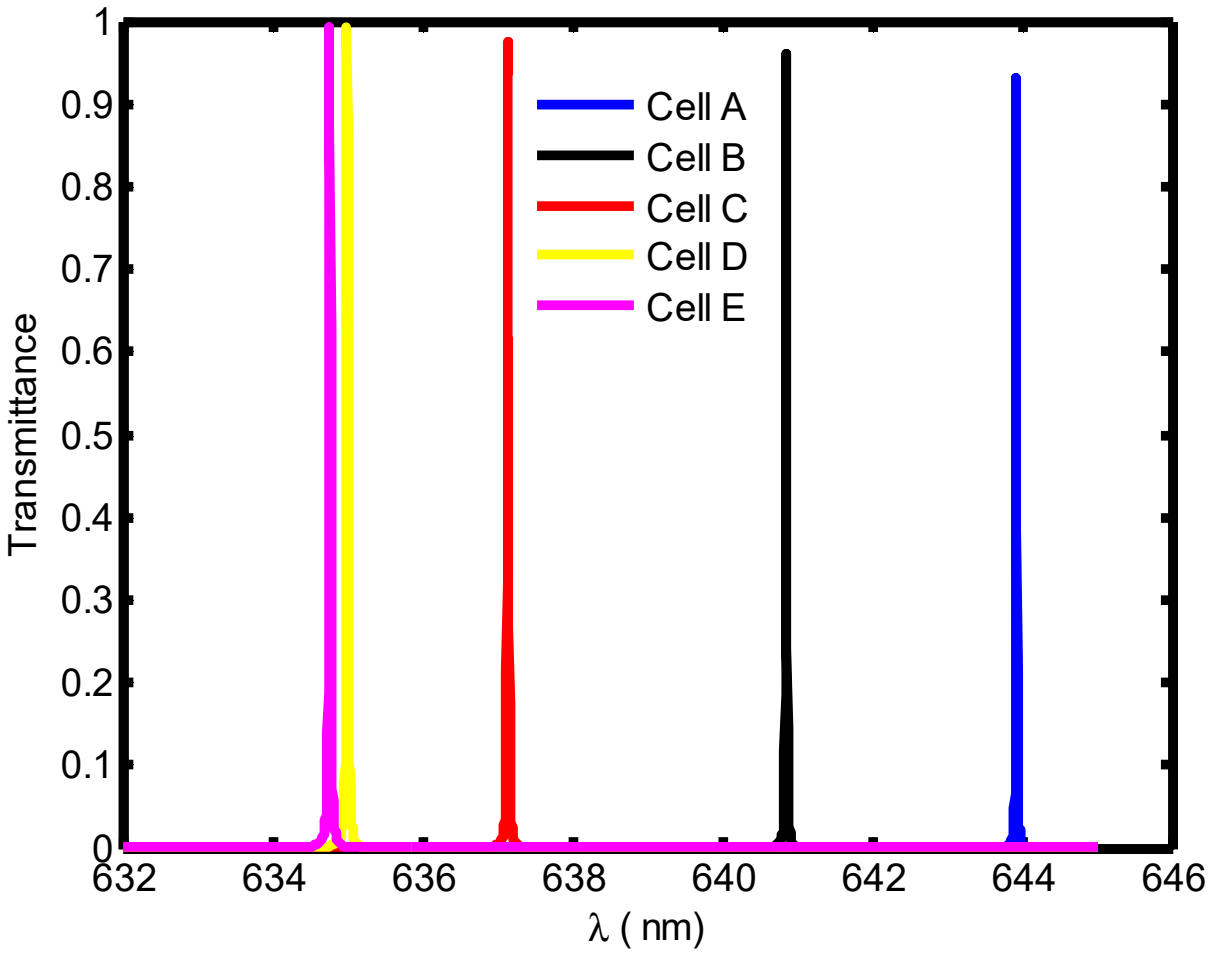

Figure 6. Transmission spectra showing five defect modes in solid blue, black, brown, yellow and purple line colors corresponding to RBC sample containing A, B, C, D and E blood cells separately, one at a time. The thickness of cavity layer is *dd* = 2200 nm under normal incidence.

Table 2. Sensitivity calculations of proposed biosensors corresponding to different defect layer thicknesses.

Defect Layer Thickness (nm)	Sensitivity (nm/RIU)
dd = 1000	141.6
dd = 2200	248.1
dd = 3000	303
dd = 5000	327.7

The data presented in Table 2 have been visualized by plotting Figure 9, which shows the dependence of sensitivity on the thickness of the defect layer region. Figure 9 shows that, as the thickness of the defect layer increases from 1000 nm to 3000 nm, the sensitivity increases linearly and reaches to 303 nm/RIU. Further increase in the thickness of thedefect layer results in a relatively small change in the sensitivity, as shown in Figure 9. The maximum sensitivity of 327.7 nm/RIU is reached, corresponding to a defect layer thickness of 5000 nm. Thus, a defect layer thickness of 5000 nm can be considered as an optimum value of thickness under which our design becomes highly sensitive. Additionally, corresponding to the optimum value of defect layer thickness, our design is capable of detecting very minute changes in the refractive index of RBC samples containing Cell B to Cell E with respect to Cell A.

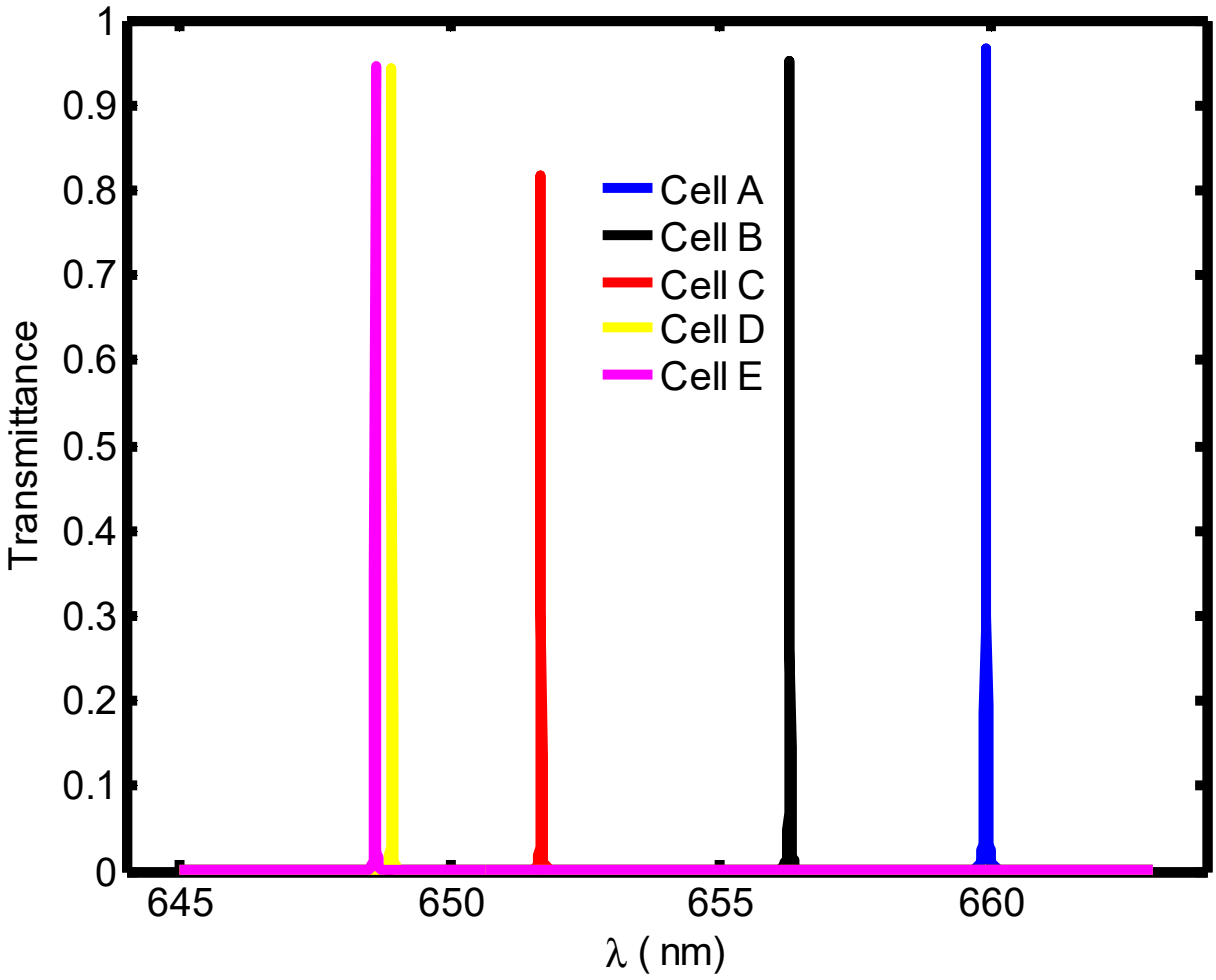

Figure 7. Transmission spectra showing five defect modes in solid blue, black, brown, yellow and purple line colors corresponding to RBC sample containing A, B, C, D and E blood cells separately, one at a time. The thickness of cavity layer is *dd* = 3000 nm under normal incidence.

4.4. Evaluation of the Performance of Proposed Biosensors Corresponding to Optimum Cavity Thickness under Normal Incidence

Apart from sensitivity, we have also examined to figure of merit (FoM) and quality factor (QF) values of proposed malaria sensors in true sense. These two parameters are also important while evaluating the working efficiency of any photonic biosensor. Mathematically, we can define FoM and QF with the help of following expressions as [6–11]

$$QF = \frac{\lambda_{peak}}{\lambda_{FWHM}} \tag{6}$$

$$FoM = \frac{S}{\lambda_{FWHM}} \tag{7}$$

To conclude our work, we have evaluated the *S*, *FoM* and *QF* of the proposed design under optimum cavity thickness of 5000 nm. The numeric values of S, FoM and QF of the proposed design, loaded with RBC samples containing Cell B, Cell C, Cell D and Cell E with respect to Cell A, are listed in Table 3 below.

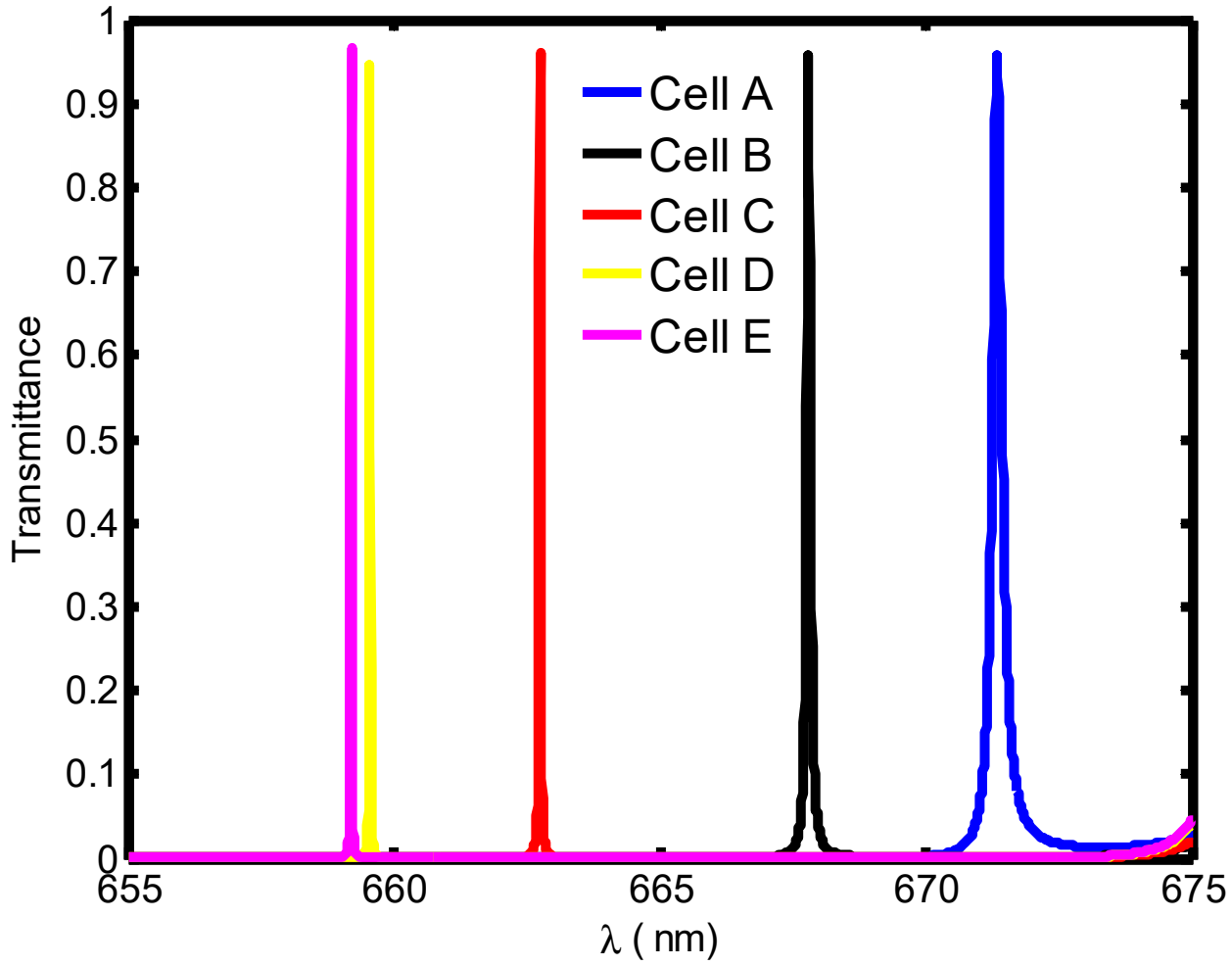

Figure 8. Transmission spectra showing five defect modes in solid blue, black, brown, yellow and purple line colors corresponding to RBC sample containing A, B, C, D and E blood cells separately, one at a time. The thickness of cavity layer is *dd* = 5000 nm under normal incidence.

Table 3. Performance evaluation table showing the numeric values of sensitivity, full width half maximum, figure of merit and quality factor of the proposed biosensor, corresponding to different RBC components under optimum condition.

Blood Component	Refractive Index	λ_{Peak} (nm)	S (nm/RIU)	λ_{FWHM} (nm)	FoM	QF
Cell A	1.408	671.4	—	0.11	—	6103.63
Cell B	1.396	667.8	300	0.036	8333.3	18550
Cell C	1.381	662.7	322.2	0.0135	23,866.7	49,088.8
Cell D	1.372	659.6	327.7	0.01	32,770	65960
Cell E	1.371	659.2	310.5	0.0095	32,684.2	69,389.47

It can easily be observed from the data in Table 3 that the sensitivity of the proposed biosensor varies between a maximum of 327.7 nm/RIU to a minimum of 300 nm/RIU when the cavity is infiltrated with RBC samples containing cell D and cell B, respectively. On the other hand, FoM and QF values vary between 2.3×10^4 to 8.33×10^3 and 6.93×10^4 to 1.85×10^4, respectively, depending upon the nature of malaria samples with respect to the water sample. Under the light of the above facts, we have come to the conclusion that our proposed design can be efficiently used for the detection of malaria infection from the preliminary stage (ring stage) to advanced stage (schizont stage).

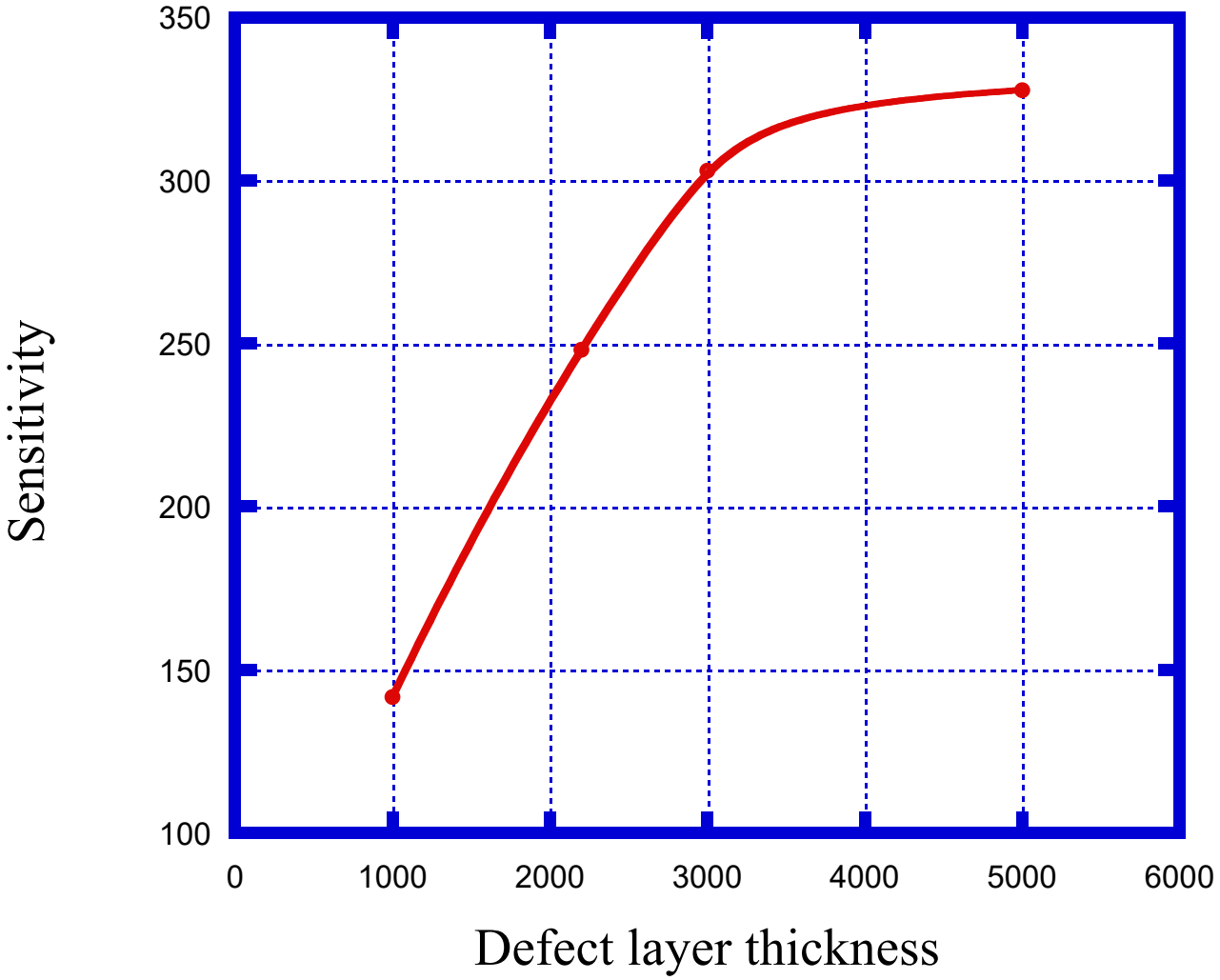

Figure 9. Variation of sensitivity with respect to defect layer thickness.

Finally, we have given our efforts to compare the findings of a proposed blood sensor for malaria detection with the similar kind of work based on various blood sensing applications. This comparison has been presented in Table 4, which highlights the blood sensing applications of various biosensors based on the principle of the refractive index sensing mechanism. This comparison shows that the proposed biosensor is suitable for sensing and detecting malaria infection from preliminary to advanced stages effectively. The dependence of our design on photonic biosensing technology makes it suitable for obtaining rapid, accurate and timely reports to ensure proper diagnosis, treatment and cure.

Table 4. Comparison of sensitivity, figure of merit and quality factor values of proposed 1D photonic blood sensor for malaria sensing and detection with similar kinds of work of other researchers at normal incidence (NR = Not reported).

Year	Structure Details	Type of Analyte	S	FoM	QF	Reference
2019	1D PC with graphene coated cavity walls	Blood plasma	51.49 nm/RIU	NR	NR	[55]
2019	2D PC waveguide structure	10 different blood components	473.38	7324.2	NR	[56]
2019	D shaped PC fiber	Blood glucose	0.83	NR	NR	[57]
2020	1D PC without coated cavity walls	Blood hemoglobin	141	0.48	NR	[58]
This work	1D PC without coated cavity walls	Red blood cells	327.7	32770	69,389.47	—

5. Conclusions

In the present piece of theoretical research work, we have explored the sensing and detection capabilities of 1D PC with defect for investigating malaria infection from preliminary to advanced stage by examining the different samples containing red blood cells A, B, C, D and E. We have used a transfer matrix formulation under normal incidence condition and MATLAB simulation software to obtain the results pertaining to the work. This study has been carried out on the five structures of different cavity layer thicknesses set as 1000 nm, 2200 nm, 3000 nm and 5000 nm to identify the structure having optimum biosensing performance. Our study shows that the biosensing performance of design maximizes corresponding to cavity thickness 5000 nm. The maximum sensitivity value obtained from this structure is 327.7 nm/RIU when the cavity is infiltrated with the RBC sample containing Cell D, which corresponds with the Schizont stage of malaria infection. Thus, our design can be very useful for identifying the person affected with different stages of malaria infection due to accuracy in the results. Additionally, the proposed work is based on minute sensing of the refractive index of different RBC samples of variation 1.408 to 1.371 corresponding to hemoglobin concentration 30.9g/dL to 15.9 g/dL, respectively. The maximum values of figure of merit and quality factor of proposed biosensing design are 32,770 RIU and 69,389.7, respectively, which is high as expected.

Author Contributions: The software handling, results preparation, investigation and initial manuscript draft preparation have been carried out by S.K.S. Conceptualization, methodology, reviewing, editing and supervision have been carried out by S.K.A. All authors have read and agreed to the published version of the manuscript.

Funding: There is no funding for the present work.

Institutional Review Board Statement: Not applicable.

Informed Consent Statement: Not applicable.

Data Availability Statement: It is not applicable to the present manuscript. The results of the present theoretical work are based on MATLAB simulations. All the relations and other relevant information have been properly cited throughout the manuscript, keeping the ease of readers of the journal. The readers can easily reproduce the results of the work with the help of theoretical details given in the manuscript, with the help of MATLAB computational software.

Conflicts of Interest: Authors do not have any conflict of interest.

References

1. Yablonovitch, E. Inhibited Spontaneous Emission in Solid-State Physics and Electronics. *Phys. Rev. Lett.* **1987**, *58*, 2059–2062. [CrossRef] [PubMed]
2. John, S. Strong localization of photons in certain disordered dielectric superlattices. *Phys. Rev. Lett.* **1987**, *58*, 2486–2489. [CrossRef] [PubMed]

3. Awasthi, S.K.; Mishra, A.; Malaviya, U.; Ojha, S. Wave propagation in a one-dimensional photonic crystal with metamaterial. *Solid State Commun.* **2009**, *149*, 1379–1383. [CrossRef]
4. Awasthi, S.K.; Malaviya, U.; Ojha, S.P. Enhancement of omnidirectional total-reflection wavelength range by using one-dimensional ternary photonic bandgap material. *J. Opt. Soc. Am. B* **2006**, *23*, 2566–2571. [CrossRef]
5. Danaie, M.; Kiani, B. Design of a label-free photonic crystal refractive index sensor for biomedical applications. *Photon-Nanostructures—Fundam. Appl.* **2018**, *31*, 89–98. [CrossRef]
6. Aly, A.H.; Awasthi, S.K.; Mohaseb, M.A.; Matar, Z.S.; Amin, A.F. MATLAB Simulation-Based Theoretical Study for Detection of a Wide Range of Pathogens Using 1D Defective Photonic Structure. *Crystals* **2022**, *12*, 220. [CrossRef]
7. Aly, A.H.; Awasthi, S.K.; Mohamed, D.; Matar, Z.S.; Al-Dossari, M.; Amin, A.F. Study on a one-dimensional defective photonic crystal suitable for organic compound sensing applications. *RSC Adv.* **2021**, *11*, 32973–32980. [CrossRef] [PubMed]
8. Aly, A.H.; Awasthi, S.K.; Mohamed, A.M.; Matar, Z.S.; Mohaseb, M.A.; Al-Dossari, M.; Tammam, M.T.; Zaky, Z.A.; Amin, A.F.; Sabra, W. Detection of Reproductive Hormones in Females by Using 1D Photonic Crystal-Based Simple Reconfigurable Biosensing Design. *Crystals* **2021**, *11*, 1533. [CrossRef]
9. Zaky, Z.A.; Moustafa, B.; Aly, A.H. Plasma cell sensor using photonic crystal cavity. *Opt. Quantum Electron.* **2021**, *53*, 591. [CrossRef]
10. Elsayed, A.M.; Ahmed, A.M.; Aly, A.H. Glucose sensor modeling based on Fano resonance excitation in titania nanotube photonic crystal coated by titanium nitride as a plasmonic material. *Appl. Opt.* **2022**, *61*, 1668. [CrossRef]
11. Mehaney, A.; Abadla, M.M.; Elsayed, H.A. 1D porous silicon photonic crystals comprising Tamm/Fano resonance as high performing optical sensors. *J. Mol. Liq.* **2021**, *322*, 114978. [CrossRef]
12. Troia, B.; Paolicelli, A.; De, F.; Passaro, V.M.N. Photonic Crystals for Optical Sensing: A Review. In *Advances in Photonic Crystals*; IntechOpen: Rijeka, Croatia, 2013. [CrossRef]
13. Zhou, X.; Zhang, L.; Armani, A.M.; Liu, J.; Duan, X.; Zhang, D.; Zhang, H.; Pang, W. An Integrated Photonic Gas Sensor Enhanced by Optimized Fano Effects in Coupled Microring Resonators With an Athermal Waveguide. *J. Light. Technol.* **2015**, *33*, 4521–4530. [CrossRef]
14. Bougriou, F.; Bouchemat, T.; Bouchemat, M.; Paraire, N. Optofluidic sensor using two-dimensional photonic crystal waveguides. *Eur. Phys. J. Appl. Phys.* **2013**, *62*, 11201. [CrossRef]
15. Pursiainen, O.L.J.; Baumberg, J.J.; Ryan, K.; Bauer, J.; Winkler, H.; Viel, B.; Ruhl, T. Compact strain-sensitive flexible photonic crystals for sensors. *Appl. Phys. Lett.* **2005**, *87*, 101902. [CrossRef]
16. Roggan, A.; Friebel, M.; Dörschel, K.; Hahn, A.; Müller, G. Optical Properties of Circulating Human Blood in the Wavelength Range 400–2500 nm. *J. Biomed. Opt.* **1999**, *4*, 36–46. [CrossRef]
17. A Report by the World Economic Forum and the Harvard School of Public Health. September 2011. Available online: www.weforum.org/EconomicsOfNCDappendix (accessed on 1 September 2019).
18. Lee, V.S.; Tarassenko, L. Absorption and multiple scattering by suspensions of aligned red blood cells. *J. Opt. Soc. Am. A* **1991**, *8*, 1135–1141. [CrossRef] [PubMed]
19. Zhernovaya, O.; Sydoruk, O.; Tuchin, V.; Douplik, A. The refractive index of human hemoglobin in the visible range. *Phys. Med. Biol.* **2011**, *56*, 4013–4021. [CrossRef]
20. Bayer, R.; Çağlayan, S.; Guenther, B. Discrimination between orientation and elongation of RBC in laminar flow by means of laser diffraction. *Proc. SPIE* **1994**, *2136*, 105–114. [CrossRef]
21. Prahl, S.A. 1999. Available online: http://omlc.ogi.edu/spectra/hemoglobin/index.html (accessed on 1 September 2019).
22. Enejder, A.M.K.; Swartling, J.; Aruna, P.; Andersson-Engels, S. Influence of cell shape and aggregate formation on the optical properties of flowing whole blood. *Appl. Opt.* **2003**, *42*, 1384–1394. [CrossRef]
23. Lindberg, L.-G.; Öberg, P. Optical properties of blood in motion. *Opt. Eng.* **1993**, *32*, 253–257. [CrossRef]
24. Sharma, P.; Sharan, P. Design of photonic crystal based ring resonator for detection of different blood constituents. *Opt. Commun.* **2015**, *348*, 19–23. [CrossRef]
25. Tangpukdee, N.; Duangdee, C.; Wilairatana, P.; Krudsood, S. Malaria Diagnosis: A Brief Review. *Korean J. Parasitol.* **2009**, *47*, 93–102. [CrossRef] [PubMed]
26. Gentilini, M. Maladies parasitaires. In *MédecineTropicale*, 5th ed.; 2ème Tirage Actualisé; Flammarion Médecine Science: Paris, France, 1995; pp. 51–122. Available online: https://www.decitre.fr/livres/medecine-tropicale-9782257143945.html (accessed on 1 September 2019).
27. WHO Report. 2019. Available online: https://www.who.int/malaria/publications/world-malaria-report-2019/en/ (accessed on 1 September 2019).
28. Agnero, M.A.; Konan, K.; Tokou, Z.G.C.S.; Kossonou, Y.T.A.; Dion, B.S.; Kaduki, K.A.; Zoueu, J.T. Malaria-Infected Red Blood Cell Analysis through Optical and Biochemical Parameters Using the Transport of Intensity Equation and the Microscope's Optical Properties. *Sensors* **2019**, *19*, 3045. [CrossRef]
29. Erdman, L.K.; Kain, K.C. Molecular diagnostic and surveillance tools for global malaria control. *Travel Med. Infect. Dis.* **2008**, *6*, 82–99. [CrossRef] [PubMed]
30. Bell, D.; Wongsrichanalai, C.; Barnwell, J.W. Ensuring quality and access for malaria diagnosis: How can it be achieved? *Nat. Rev. Genet.* **2006**, *4*, S7–S20. [CrossRef]

31. E Clendennen, T.; Long, G.W.; Baird, J.K.; Iii, T.E.C. QBC® and Giemsa-stained thick blood films: Diagnostic performance of laboratory technologists. *Trans. R. Soc. Trop. Med. Hyg.* **1995**, *89*, 183–184. [CrossRef]
32. Shaheen, S.A.; Taya, S.A. Propagation of p-polarized light in photonic crystal for sensor application. *Chin. J. Phys.* **2017**, *55*, 571–582. [CrossRef]
33. Sovizi, M.; Aliannezhadi, M. Design and simulation of high-sensitivity refractometric sensors based on defect modes in one-dimensional ternary dispersive photonic crystal. *J. Opt. Soc. Am. B* **2019**, *36*, 3450–3456. [CrossRef]
34. Taya, S. Ternary photonic crystal with left-handed material layer for refractometric application. *Opto-Electronics Rev.* **2018**, *26*, 236–241. [CrossRef]
35. Banerjee, A. Design of enhanced sensitivity gas sensors by using 1D defect ternary photonic band gap structures. *Indian J. Phys.* **2019**, *94*, 535–539. [CrossRef]
36. Xie, Q.; Chen, Y.; Li, X.; Yin, Z.; Wang, L.; Geng, Y.; Hong, X. Characteristics of D-shaped photonic crystal fiber surface plasmon resonance sensors with different side-polished lengths. *Appl. Opt.* **2017**, *56*, 1550–1555. [CrossRef]
37. Zhang, Z.; Shen, T.; Wu, H.; Feng, Y.; Wang, X. Polished photonic crystal fiber refractive index sensor based on surface plasmon resonance. *J. Opt. Soc. Am. B* **2021**, *38*, F61. [CrossRef]
38. Nie, T.; Han, Z.; Gou, Z.; Wang, C.; Tian, H. High anti-interference dual-parameter sensor using EIT-like effect photonic crystal cavity coupled system. *Appl. Opt.* **2022**, *61*, 1552–1558. [CrossRef] [PubMed]
39. Baraket, Z.; Soltani, O.; Kanzari, M. Design of magnetic field direction's sensor based on a 1D tunable magneto-photonic crystal. *Opt. Quantum Electron.* **2022**, *54*, 637. [CrossRef]
40. Parandin, F.; Heidari, F.; Aslinezhad, M.; Parandin, M.M.; Roshani, S.; Roshani, S. Design of 2D photonic crystal biosensor to detect blood components. *Opt. Quantum Electron.* **2022**, *54*, 618. [CrossRef]
41. Parandin, F.; Heidari, F.; Rahimi, Z.; Olyaee, S. Two-Dimensional photonic crystal Biosensors: A review. *Opt. Laser Technol.* **2021**, *144*, 107397. [CrossRef]
42. Liu, Y.; Salemink, H.W.M. Photonic crystal-based all-optical on-chip sensor. *Opt. Express* **2012**, *20*, 19912–19920. [CrossRef]
43. Olyaee, S.; Dehghani, A.A. Ultrasensitive Pressure Sensor Based on Point Defect Resonant Cavity in Photonic Crystal. *Sens. Lett.* **2013**, *11*, 1854–1859. [CrossRef]
44. Pacholski, C. Photonic Crystal Sensors Based on Porous Silicon. *Sensors* **2013**, *13*, 4694–4713. [CrossRef]
45. Matar, Z.S.; Al-Dossari, M.; Awasthi, S.K.; El-Gawaad, N.S.A.; Hanafy, H.; Amin, R.M.; Fathy, M.I.; Aly, A.H. Theoretical Study on Polycarbonate-Based One-Dimensional Ternary Photonic Structures from Far-Ultraviolet to Near-Infrared Regions of Electromagnetic Spectrum. *Crystals* **2022**, *12*, 642. [CrossRef]
46. Del Villar, I.; Matias, I.R.; Arregui, F.J.; Claus, R. Analysis of one-dimensional photonic band gap structures with a liquid crystal defect towards development of fiber-optic tunable wavelength filters. *Opt. Express* **2003**, *11*, 430–436. [CrossRef] [PubMed]
47. Saravanan, S.; Dubey, R. Optical and morphological studies of TiO2 nanoparticles prepared by sol–gel method. *Mater. Today: Proc.* **2021**, *47*, 1811–1814. [CrossRef]
48. Awasthi, S.K.; Panda, R.; Shiveshwari, L. Multichannel tunable filter properties of 1D magnetized ternary plasma photonic crystal in the presence of evanescent wave. *Phys. Plasmas* **2017**, *24*, 072111. [CrossRef]
49. Awasthi, S.K.; Panda, R.; Chauhan, P.K.; Shiveshwari, L. Multichannel tunable omnidirectional photonic band gaps of 1D ternary photonic crystal containing magnetized cold plasma. *Phys. Plasmas* **2018**, *25*, 052103. [CrossRef]
50. Ankita; Suthar, B.; Bhargava, A. Biosensor Application of One-Dimensional Photonic Crystal for Malaria Diagnosis. *Plasmonics* **2020**, *16*, 59–63. [CrossRef]
51. Agnero, M.A.; Konan, K.; Kossonou, A.T.; Bagui, O.K.; Zoueu, J.T. A New Method to Retrieve the Three-Dimensional Refractive Index and Specimen Size Using the Transport Intensity Equation, Taking Diffraction into Account. *Appl. Sci.* **2018**, *8*, 1649. [CrossRef]
52. Mazeron, P.; Muller, S.; Elazouzi, H. Deformation of erythrocytes under shear: A small-angle light scattering study. *Biorheology* **1997**, *34*, 99–110. [CrossRef]
53. Phillips, K.G.; Jacques, S.L.; Mccarty, O.J.T. Measurement of Single Cell Refractive Index, Dry Mass, Volume, and Density Using a Transillumination Microscope. *Phys. Rev. Lett.* **2012**, *109*, 118105. [CrossRef]
54. Tycko, D.H.; Metz, M.H.; Epstein, E.A.; Grinbaum, A. Flow-cytometric light scattering measurement of red blood cell volume and hemoglobin concentration. *Appl. Opt.* **1985**, *24*, 1355. [CrossRef]
55. El-Khozondar, H.J.; Mahalakshmi, P.; El-Khozondar, R.J.; Ramanujam, N.; Amiri, I.; Yupapin, P. Design of one dimensional refractive index sensor using ternary photonic crystal waveguide for plasma blood samples applications. *Phys. E: Low-Dimensional Syst. Nanostructures* **2019**, *111*, 29–36. [CrossRef]
56. Mohammed, N.A.; Hamed, M.M.; Khalaf, A.A.; Alsayyari, A.; El-Rabaie, S. High-sensitivity ultra-quality factor and remarkable compact blood components biomedical sensor based on nanocavity coupled photonic crystal. *Results Phys.* **2019**, *14*, 102478. [CrossRef]

57. Lidiya, A.E.; Raja, R.V.J.; Pham, V.D.; Ngo, Q.M.; Vigneswaran, D. Detecting hemoglobin content blood glucose using surface plasmon resonance in D-shaped photonic crystal fiber. *Opt. Fiber Technol.* **2019**, *50*, 132–138. [CrossRef]
58. Abadla, M.M.; Elsayed, H.A. Detection and sensing of hemoglobin using one-dimensional binary photonic crystals comprising a defect layer. *Appl. Opt.* **2020**, *59*, 418–424. [CrossRef] [PubMed]